Journal of Structural Geology, Vol. 15, Nos 3–5, pp. 277 to 291, 1993
Printed in Great Britain

0191-8141/93 $06.00 + 0.00

Effects of the superposition of compaction and tectonic strain during folding of a multilayer sequence—model and observations

STEFANO MAZZOLI and SABINA CARNEMOLLA

Geologisches Institut, ETH-Zentrum, Sonneggstrasse 5, CH-8092 Zürich, Switzerland

(*Received* 4 *January* 1992; *accepted in revised form* 28 *July* 1992)

Abstract—Sedimentary rocks deformed at shallow crustal depth can show a wide variety of planar, linear and mixed planar–linear fabrics depending on their structural position within folds. A model has been developed which tries to explain this variation in fabric development in terms of the strain states that it represents. We analyse the finite strain states that may develop during compaction and subsequent buckle folding of sedimentary multilayers composed of a regular alternation of competent and incompetent beds. The geometric properties of the multilayer during buckling have been analysed from a finite element model characterized by: linear viscous material properties, a viscosity contrast $\mu_1/\mu_2 = 40$, and a ratio of incompetent to competent layer thickness $d_2/d_1 = 1$. Sequential matrix multiplication allows the determination of the finite strain states for all stages of fold development.

Finite strain states predicted from the model appear to be in good agreement with observations of fabric development in naturally deformed rocks from the Southern Apennines. During progressive deformation in the model, the finite strain ellipsoid in the limb regions of folded incompetent layers is consistently oblate, and the XY plane lies at a small angle to bedding as a consequence of previous compaction. Natural cleavage consistently lies at a low angle to bedding in folded argillites from the Southern Apennines and it can be interpreted to represent the XY plane of the total finite strain ellipsoid in strongly compacted sediments, and not that of tectonic deformation alone.

In the hinge regions of open folds, finite strains predicted in the incompetent layers of the model are of prolate type, and they become oblate as the interlimb angle decreases; the presence of a 'true' pencil structure in open folds and of a spaced cleavage associated with a 'regular' pencil structure in more close folds, often noted in the case study of the Southern Apennines, most probably reflects this change from prolate to oblate strain in the hinge zones as folding proceeds.

INTRODUCTION

FABRIC development in sedimentary rocks deformed at shallow crustal depth is controlled by several parameters including structural position, together with rock composition and deformational environment (e.g. Engelder & Marshak 1985). Such rocks can display a wide variety of planar and linear fabrics, ranging from well-developed slaty cleavage, to weakly formed cleavage crossing the bedding, to bedding–cleavage intersection pencil structures, to irregular pencil structures showing no distinct planar fabric anisotropies (e.g. Ramsay & Huber 1983, pp. 185–188). A certain lithology within individual folds may show planar fabrics in some parts, and linear or mixed planar–linear fabrics in other parts. A spatial variation in the finite strain states within folds must account for this fabric variation. The aim of this study is to analyse the finite strains that are likely to develop in different parts of multilayer folds in order to assist the interpretation of the observed variation in fabric development. It is well known that finite strain in naturally deformed rocks of sedimentary origin may result from the superposition of tectonic distortion on diagenetic compaction. The form of deformed objects in rocks may be used to more or less approximate the total strain resulting from this superposition, depending on the sensitivity of the strain indicators to compaction. In any case, this superposition may have a major influence on fabric development, especially in argillaceous lithologies (e.g. Engelder & Geiser 1979, Reks & Gray 1982, Ramsay & Huber 1983, pp. 185–188). According to Ramsay & Wood (1973), this superposition may account for the predominance of oblate strains recorded from slaty rocks.

In the present study, we focus mainly on the finite strain states that may arise from the superposition of tectonic plane strain on uniaxial compaction during folding of a multilayer sequence. Tectonic plane strain is used in the model since it represents a simple type of tectonic deformation which is believed to be common in nature (Sanderson 1976). In the last part of the paper the features predicted from the model are compared to actual fabric development in deformed Lower Cretaceous sediments outcropping in the Lagonegro tectonic window of the Southern Apennines (Italy). The parameters (i.e. straining factors) used in the model were initially decided on the basis of field observations on these rocks.

GEOLOGICAL SETTING OF FIELD STUDY AREA

The Mesozoic sequence of the Lagonegro Basin outcrops mainly in the Lucania region southeast of Naples (Fig. 1) within the series of thrust nappes that form the South Apennine chain. In the Lagonegro area (Fig. 1), basin sediments represented by Upper Triassic cherty limestones, Jurassic radiolarian cherts and Lower Cretaceous interbedded shales and limestones are exposed

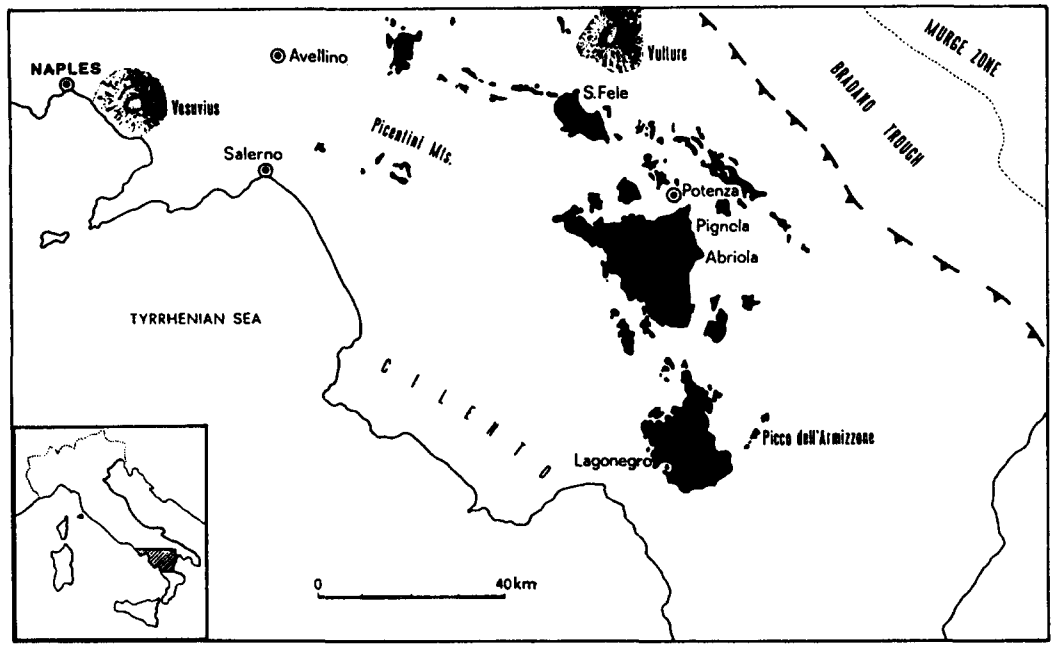

Fig. 1. Distribution of the principal outcrops of the Lagonegro Basin Mesozoic sequence of the Southern Apennines (from Scandone 1975). Study area is represented by the southernmost dark area on the map (Lagonegro tectonic window).

through a tectonic window in the overlying carbonate platform and transitional units (Scandone 1972). The Mesozoic basin sequence has been deformed by one major period of Miocene deformation, leading to folding and thrusting with a general eastern vergence. A later period of deformation produced minor refolding at a high angle to the already formed structures. Metamorphic grade in this area is in the anchizone field (Pozzuoli *et al.* 1977). A large variety of F_1 folds (from open, upright folds to isoclinal, recumbent folds) have been developed in this multilayer sequence as a result of a deformation dominated by shear-induced buckle folding. The rocks analysed, representing the stratigraphically higher part of the sequence, belong to the Lower Cretaceous Galestri Formation (Scandone 1975). It consists of a 400–500 m thick monotonous alternation of dark argillites and strongly siliceous limestones. At the contact between argillite and limestone beds cone-in-cone structures are often found, typically formed during diagenesis by calcite cement growth during vertical compaction. Mesoscopic (F_1) folds within this unit are open to tight, with half wavelengths of 0.5–10 m and amplitudes of 0.5–6 m. Fold geometry alternates between class 1 and class 3 (Ramsay 1967). Competent limestone layers have rounded hinges and show class 1b or class 1c geometries. Less competent argillites have angular to rounded hinges and typically exhibit class 3 geometries. Fold shape varies from symmetric and upright to asymmetric and overturned, with interlimb angles ranging from 12° to 95°. The geometry of the folded multilayer closely resembles that of model D of Ramsay & Huber (1987, pp. 414–418), which is characterized by high ductility contrast and high ratio of incompetent to competent layers. In such a multilayer, compression leads rapidly to the formation of buckles, the system undergoing very little layer-parallel shortening. This is confirmed in the field by the absence of cleavage fanning around folded competent beds, that would be expected if consistent homogeneous layer-parallel shortening preceded fold development. Only in the hinge region of tight folds can a spaced dissolution cleavage, roughly perpendicular to the stratification, be observed in the inner arc of the competent layers. Strain measurements on the fold profile (carried out by R_f/ϕ shape analysis on deformed radiolarians) show a maximum shortening direction approximately normal to bedding. These determinations indicate that fossil distortion accompanied compaction in the competent beds and that tectonic layer-parallel shortening has not been large enough to reverse pre-tectonic strain. Also, they show a lack of consistent layer-parallel shear within the competent strata. All these features suggest that buckling was mainly accommodated in the competent layers by tangential longitudinal strain.

THE MODEL

The model presented in this study analyses the finite strain states that may develop during compaction and subsequent buckle folding of sedimentary multilayers composed of a regular alternation of competent and incompetent beds. In setting up such a model, a number of assumptions have been made. The deformation of the multilayer is described by means of deformation gradient tensors representing ideal strains. Only specific parts of the deforming body are analysed, where the use of simple straining factors can approximate the actual strain fields.

Different incremental strains are assumed to act simultaneously in each part of the deforming body analysed in the model. For every considered strain increment, the total incremental strain matrix is determined by the product of the deformation gradient tensors

representing the different incremental strains. The total finite strain matrix for a given stage of the progressive deformation is obtained by the sequential multiplication of all the incremental strain matrices. In the calculations, reference axes are chosen so that the xy plane lies parallel to the layering (Fig. 2). During folding, the co-ordinate reference frame is kept fixed with respect to bedding, with the y axis parallel to the fold axis. Since plane strain conditions are assumed (no stretch is allowed along the y direction), the deformation gradient tensors can be simplified into 2×2 matrices in the strain calculations in the xz plane. For all the considered deformation increments, the principal finite extensions (e_1, e_2) and their orientations in the xz plane are obtained from the total two-dimensional strain matrix:

$$D = \begin{bmatrix} a & b \\ c & d \end{bmatrix}. \quad (1)$$

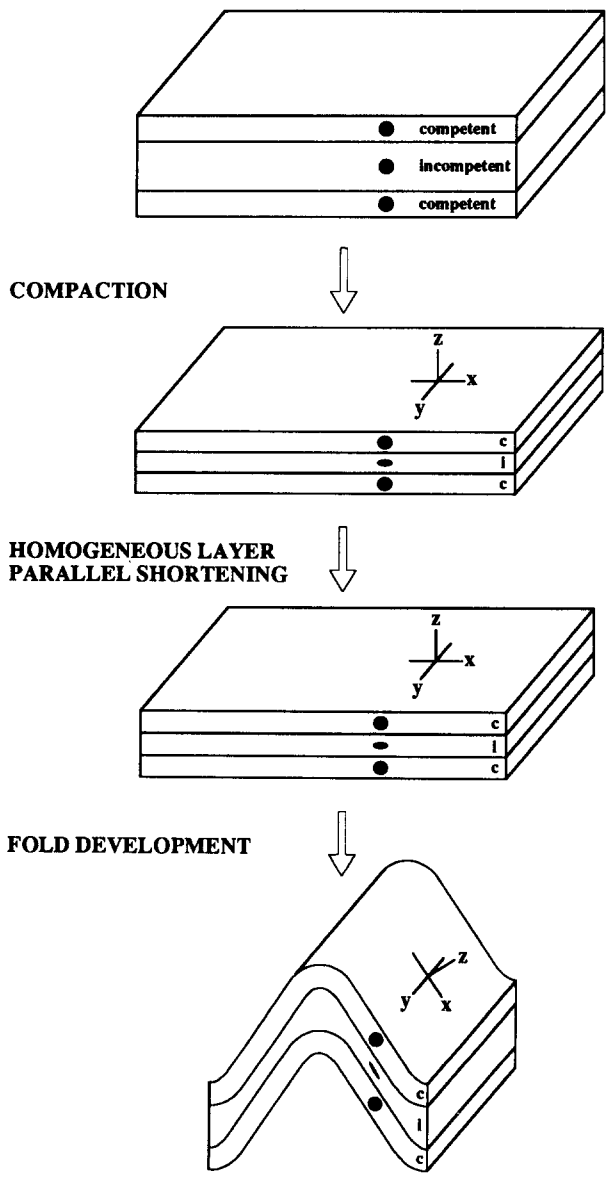

Fig. 2. Stages of deformation considered in the model. Note the co-ordinate reference frame (kept fixed with respect to layering during folding, with the y axis parallel to the fold axis).

Using the equations (from Ramsay & Huber 1983, p. 287):

$$(1 + e_1) = \{1/2\{a^2 + b^2 + c^2 + d^2 + [(a^2 + b^2 + c^2 + d^2)^2 - 4(ad - bc)^2]^{1/2}\}\}^{1/2} \quad (2a)$$

$$(1 + e_2) = \{1/2\{a^2 + b^2 + c^2 + d^2 - [(a^2 + b^2 + c^2 + d^2)^2 - 4(ad - bc)^2]^{1/2}\}\}^{1/2} \quad (2b)$$

$$R = (1 + e_1)/(1 + e_2) \quad (2c)$$

$$\tan 2\theta' = 2(ac + bd)/(a^2 - b^2 + c^2 - d^2), \quad (2d)$$

where R is the ellipticity of the finite strain ellipse, and θ' is the angle between the long axis of this ellipse and the x axis after deformation.

Volume change during diagenetic compaction

Compaction occurs during the burial of a sedimentary sequence consisting of alternating sandy–silty and argillaceous beds. These lithologies are chosen to represent, respectively, competent and incompetent layers in the model.

Diagenetic compaction of siliciclastic or carbonate sands is influenced by a wide range of factors (cf. Coogan & Manus 1975, Wolf & Chilingarian 1976); in particular, the occurrence and extent of early cementation can significantly reduce the amount of compaction suffered by a sandy sediment. A 10–15% compaction of silt and sand beds has been recently documented in Cambrian–Ordovician flysch deposits comformably overlain by about 6 km of sediments in Nova Scotia (Wright & Henderson 1992). In the present study, a 10% volume reduction is assumed for the compaction of competent layers; this value can most probably be considered as a minimum for deeply buried sands and silts.

Compaction of argillaceous muds by expulsion of intergranular water occurs very rapidly down to a depth of about 500 m (shallow burial stage) and more slowly below that depth. An increase in the preferred orientation of the clay particles perpendicular to the compaction direction accompanies the continuous decrease in porosity with depth of burial, leading to the formation of a primary planar fabric (bedding plane fissility). At about 500 m depth, a clay mud with an initial porosity of 80% becomes a mudstone (or shale if fissile) with a porosity of about 30%, the total volume of the sediment having decreased by about 50%. With a further decrease of porosity in the deep burial stage, the mudstone (or shale) becomes an argillite with a porosity of only about 4–5%. The lowest level of the deep burial stage is considered to be at a depth of 10,000 m (Müller 1967). The transition from argillite to slate is the product of metamorphism and deformation. Weller (1959) pointed out that neither porosity, nor density, directly relate to the volume changes occurring in the sediment. In the compaction model of Burst (1969), based on a three-

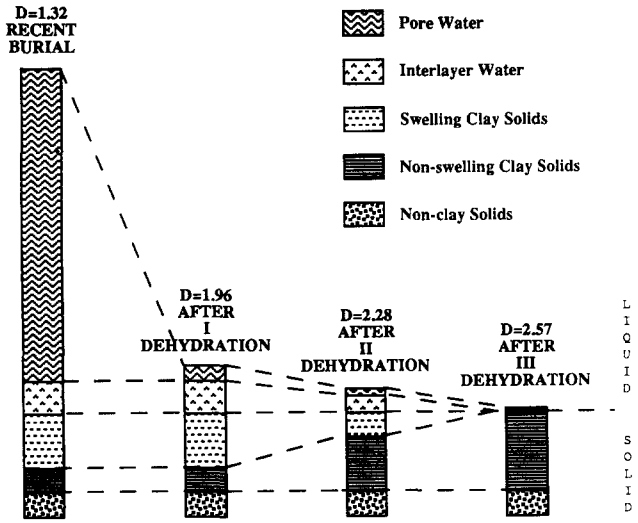

Fig. 3. Marine shale bulk composition during dehydration (from Burst 1969).

stage dehydration sequence, the change from mud–clay to argillite is accompanied by a total volume loss of 76% (Fig. 3). A volume loss of 79% is obtained by the work of Weller (1959, p. 288), which considers an originally 80% porous clayey sediment. On the other hand, a maximum initial porosity of 60% is commonly considered a good value for deltaic and marine muddy sediments (Rieke & Chilingarian 1974, p. 104). The compaction-related decrease of volume in argillaceous sediments with initial porosities in the range of 54–65% has been considered by von Engelhardt (1960) and is graphically shown in Fig. 4; the volume reduction for deeply buried argillites at, for example, 3000 m depth, ranges from 50 to 65%. In our model, we have considered the effects of two different values of volume loss due to diagenetic compaction of mud clays, in order to take into account both higher and lower amounts of volume change. The chosen values are, respectively, 78 and 55%. Within the co-ordinate system used in the present study, the deformation gradient tensor for compaction is given by:

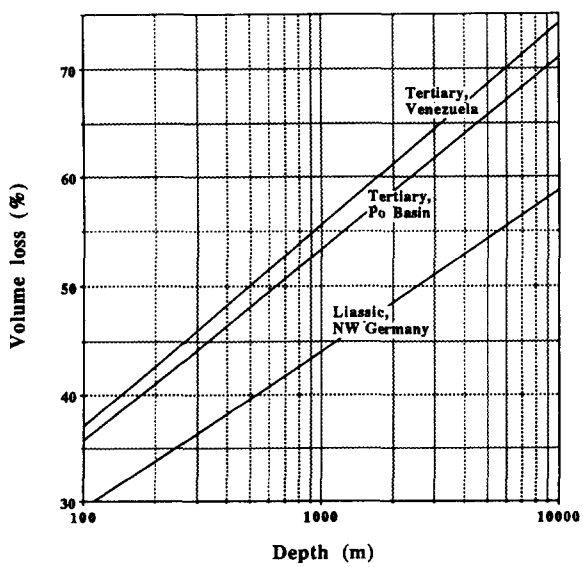

Fig. 4. Volume loss of argillaceous sediments related to depth of burial (data from von Engelhardt 1960).

$$D = \begin{matrix} 1 & 0 & 0 \\ 0 & 1 & 0 \\ 0 & 0 & (1+\Delta_0) \end{matrix} \qquad (3a)$$

or more simply in two dimensions (xz plane):

$$D = \begin{bmatrix} 1 & 0 \\ 0 & (1+\Delta_0) \end{bmatrix}, \qquad (3b)$$

where Δ_0 is the volume dilation due to compaction.

Volume change during tectonic deformation

According to Ramsay & Wood (1973) and Wood (1974), volume loss in argillaceous sediments is likely to occur also during tectonic deformation. The processes responsible for these volume changes can be schematically subdivided into two main groups: (i) processes which cause an increase in rock density, such as continued alignment and closing up of enmeshed clay particles with the expulsion of pore water and dehydration mineral transformation (clay minerals to micas); and (ii) processes which do not produce any strong density variation in the rock, such as pressure-solution transfer. Densities of undeformed, deeply buried argillites are usually in the range of 2.50–2.65 g cm^{-3} (Rieke & Chilingarian 1974, fig. 12, p. 34, Wood 1974), whereas argillaceous slates have densities of between 2.7 and 2.85 g cm^{-3} (Ramsay & Wood 1973). Structural and stratigraphic evidence shows that most argillaceous slates, at the time of deformation, were under high confining pressures with an overburden of several thousand metres; it is therefore unlikely that pre-deformational densities could be less than 2.5 g cm^{-3} (Wood 1974). On the basis of these considerations, a limit of about 10% can be assumed for the amount of volume decrease due to the group (i) processes. This amount of volume loss can be augmented by group (ii) processes. According to Ramsay & Wood (1973), the total volume loss accompanying the development of cleavage in slates is generally not greater than 20%. In particular cases, however, evidence for large (40–60%) volume loss associated with pressure solution accompanying slaty cleavage formation has been presented (Wright & Platt 1982, Beutner & Charles 1985, Wright & Henderson 1992).

In the present study, the effects of a non-constant incremental volume change is considered. The earliest stages of tectonic deformation, leading to a contraction sub-parallel to the bedding surface, are accompanied by volume loss as a result of mechanical closure of pore spaces left after diagenetic compaction and the expulsion of pore water still contained in the shale or argillite (Ramsay & Huber 1983, p. 185). As deformation proceeds, further volume loss is mainly due to dehydration mineral reactions, such as the transition from clays to micas, and to solution transfer; the incremental volume change is likely to decrease in these later stages. This effect of incremental volume change decreasing as deformation proceeds is approximated in the model using a logarithmic relation between incremental volume change and tectonic finite strain (Fig. 5).

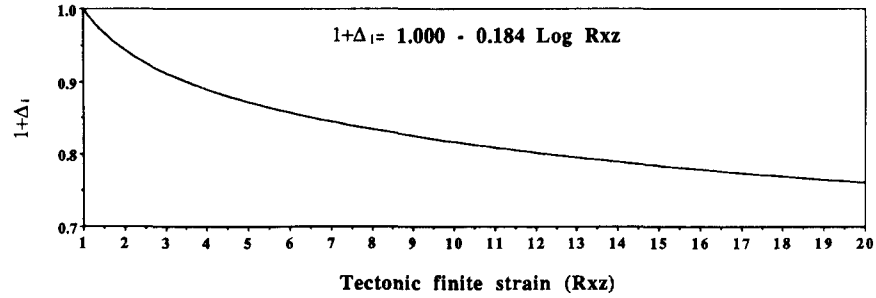

Fig. 5. Relationship between incremental volume change and tectonic deformation for the incompetent layers in the model.

In the competent layers, no volume change is assumed during tectonic deformation.

Tectonic deformation

The tectonic deformation considered in the present study arises from shortening parallel to the layering under plane strain conditions. Homogeneous layer-parallel shortening occurring before fold development is schematically considered as a separate deformation stage in the model (Fig. 2), since it produces a homogeneous strain throughout the whole multilayer. In the competent layers, the homogeneous layer contraction in the x direction is compensated by an equal amount of extension in the z direction, and the deformation matrix is given by (xz plane):

$$D = \begin{bmatrix} (1+e_1)^{-1} & 0 \\ 0 & (1+e_1) \end{bmatrix}. \quad (4)$$

In the incompetent layers, volume loss accompanies tectonic deformation. The same overall shortening as in the competent layers is imposed along the x direction, because of compatibility considerations. This results in a combination of true strain (layer-parallel shortening compensated by an equivalent vertical extension) and volume reduction along the x axis (determined from the equation of Fig. 5). The relative deformation matrix is given by:

$$D = \underbrace{\begin{bmatrix} (1 \times \Delta_i) & 0 \\ 0 & 1 \end{bmatrix}}_{\text{volume change}} \times \underbrace{\begin{bmatrix} (1+e_1)^{-1}(1+\Delta_i)^{-1} & 0 \\ 0 & (1+e_1)(1+\Delta_i) \end{bmatrix}}_{\text{layer parallel shortening}} = \begin{bmatrix} (1+e_1)^{-1} & 0 \\ 0 & (1+e_1)(1+\Delta_i) \end{bmatrix}, \quad (5)$$

where Δ_i represents the incremental dilation for the considered strain increment.

The geometric properties of the multilayer during buckling have been analysed using the finite element model of Huggenberger (1985, pp. 46–50) which is characterized by: linear viscous material properties, ratio of incompetent to competent layer thickness $d_2/d_1 = 1$, viscosity contrast $\mu_1/\mu_2 = 40$, initial wavelength to competent layer thickness ratio $\lambda/d_1 = 20$, and initial amplitude to competent layer thickness ratio $A/d_1 = 0.2$. The shape of competent and incompetent layers varies during fold development so that, as folding proceeds, they take on class 1c and class 3 shapes (Ramsay 1967), respectively, but a competent–incompetent pair as a whole maintains a similar (class 2) geometry. During fold development, finite strain states are determined for every 5° increment of fold-limb dip, for dip values from 0° up to 60°. The deformation gradient tensors applied for the deformation of the multilayer during folding are discussed separately for competent and incompetent layers.

(*a*) *Competent layers*. In the competent layers, a strain field model involving essentially no deformation in the fold limbs and tangential longitudinal strain (t.l.s.) in the hinge region is used (the change in layer thickness around a folded competent layer as it passes from class 1b to class 1c is very slight; the strain arising from the effect is negligible for the purposes of the present analysis). The strain due to t.l.s. can be determined in the xz plane from the equation (Ramsay 1967, p. 400): $R = (1 + d'/r)$, where d' = distance from the neutral surface and r = radius of curvature. The computations are made with the assumption that the neutral surface (Ramsay 1967, p. 397) does not maintain a fixed material position within the deforming layer, but that it continuously migrates in order to take up a central position in the deformed state. This assumption appears to be the most reasonable one, because it minimizes the work done in distorting the layer (Hudleston & Tabor 1988). The fold hinge is schematically subdivided into three parts: inner, mid and outer arc (Fig. 6). With the assumption made above regarding the position of the neutral surface, there is no finite deformation of the mid arc for any given folding stage. The deformation matrices for outer and inner arc, respectively, are given by:

$$D = \begin{bmatrix} (1+d'/r)^{1/2} & 0 \\ 0 & (1+d'/r)^{-1/2} \end{bmatrix} \text{ (outer arc)} \quad (6a)$$

$$D = \begin{bmatrix} (1+d'/r)^{-1/2} & 0 \\ 0 & (1+d'/r)^{1/2} \end{bmatrix} \text{ (inner arc).} \quad (6b)$$

(*b*) *Incompetent layers, limb region*. In this region, the strains set up in the model result from a combination of simple shear and pure shear components (associated

with volume changes following the relation of Fig. 5). For simplicity, the shearing parallel to layer boundaries in the fold limbs is considered directly proportional to the limb dip, as in ideal flexural folds (Ramsay 1967, p. 393). The shear strain γ is in this case equal to the angle of dip δ (expressed in radians) of the folded layer, and the deformation gradient tensor is given by:

$$D = \begin{bmatrix} 1 & \delta \\ 0 & 1 \end{bmatrix}. \quad (7)$$

The pure shear component accounts for the thinning of the limb regions of incompetent layers as they take on a class 3 shape. This deformation is accompanied by flow of incompetent material from the limbs to the hinge zones (e.g. Williams 1980). Assuming that the layer contacts on the fold limbs remain welded, this type of deformation gives rise to a complex displacement field (Fig. 7c). In the present study, the inflexion line of the fold limbs is considered (Fig. 6). This sector is assumed to behave as the central 'pin line' of the model of Fig. 7, and a pure shear strain can therefore describe the deformation of this zone. Finite strain is a simple function of limb thickness, and the deformation matrix is represented by (d_f = final layer thickness; d_i = initial layer thickness):

$$D = \begin{bmatrix} d_f/d_i & 0 \\ 0 & (d_f/d_i)^{-1} \end{bmatrix}. \quad (8)$$

The total incremental strain matrix can be obtained from the product of deformation gradient tensors (7) and (8). Since the deformation is simulated as a series of small incremental transformations, the order of pre-multiplication used to construct each incremental matrix does not substantially affect the resulting deformation history. An order of multiplication implying simple shear followed by pure shear is chosen here:

$$\underset{\text{pure shear (II)}}{\begin{bmatrix} d_f/d_i & 0 \\ 0 & (d_f/d_i)^{-1} \end{bmatrix}} \times \underset{\text{simple shear (I)}}{\begin{bmatrix} 1 & \delta \\ 0 & 1 \end{bmatrix}} = \begin{bmatrix} d_f/d_i & \delta(d_f/d_i) \\ 0 & (d_f/d_i)^{-1} \end{bmatrix}. \quad (9)$$

R_{xz} values relative to tectonic deformation alone are obtained from the equations (2) for every 5° increment

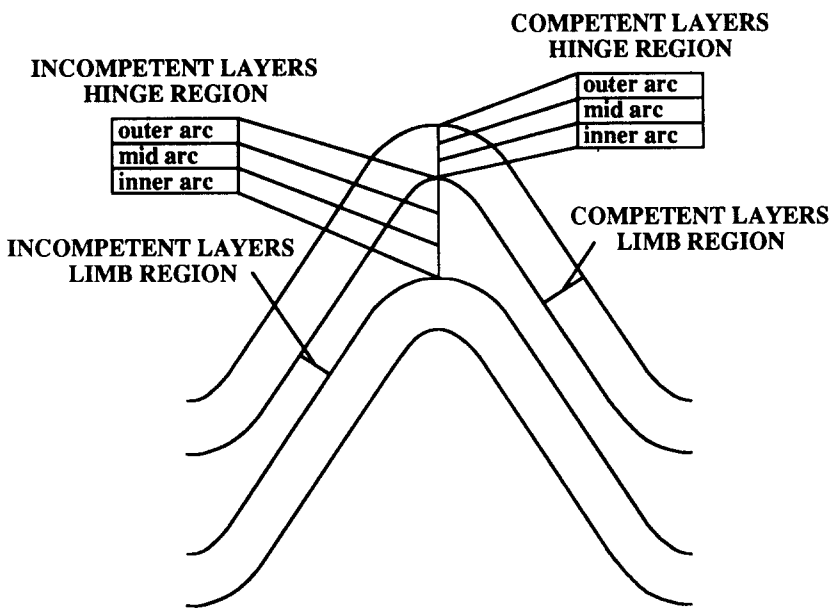

INCOMPETENT LAYERS				COMPETENT LAYERS			
LIMB REGION	HINGE REGION			LIMB REGION	HINGE REGION		
	inner arc	mid arc	outer arc		inner arc	mid arc	outer arc
COMPACTION				COMPACTION			
INITIAL L.P.S. + ΔV				INITIAL L.P.S.			
SIMPLE SHEAR + PURE SHEAR + ΔV	INVERSE T.L.S. + PURE SHEAR + ΔV	PURE SHEAR + ΔV	INVERSE T.L.S. + PURE SHEAR + ΔV		T.L.S.		T.L.S.

Fig. 6. Regions of the multilayer folds and related strain fields considered in the model (L.P.S.= homogeneous layer-parallel shortening; T.L.S.= tangential longitudinal strain; ΔV= incremental volume change during tectonic deformation).

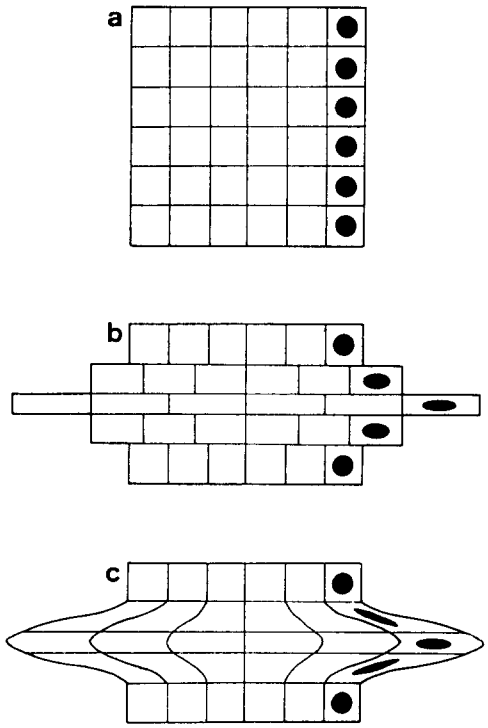

Fig. 7. Deformation by pure shear of incompetent material sandwiched between two (undeformed) competent layers. (a) Original grid. (b) Pure shear—discontinuous displacement. (c) Pure shear—continuous displacement. In (b) and (c), the vertical line in the centre of the model acts as a pin line for layer-parallel displacements (from Ramsay & Huber 1987).

of fold-limb dip; they are used for the determination of the volume changes associated with tectonic deformation by means of the equation plotted in Fig. 5. The volumetric changes are assumed to occur along the z axis of the model by displacements perpendicular to the layering. The relative deformation matrix is given by:

$$D = \begin{bmatrix} 1 & 0 \\ 0 & (1 + \Delta_i) \end{bmatrix}. \quad (10)$$

The total deformation matrix for every deformation increment can be specified by the multiplication of equations (9) and (10). Also in this case, the influence of the order of matrix multiplication on the resulting finite strain values is not substantial for the purposes of this study. The following order is adopted:

$$\begin{bmatrix} 1 & 0 \\ 0 & (1 + \Delta_i) \end{bmatrix} \times \begin{bmatrix} d_f/d_i & \delta(d_f/d_i) \\ 0 & (d_f/d_i)^{-1} \end{bmatrix} = \begin{bmatrix} d_f/d_i & \delta(d_f/d_i) \\ 0 & (1 + \Delta_i)(d_f/d_i)^{-1} \end{bmatrix}. \quad (11)$$

(*c*) *Incompetent layers, hinge region.* In this region, the simple shear component due to flexural flow is zero, and only coaxial strains are considered in the model. As in the competent layers, this region has been subdivided into three parts (inner, mid and outer arc; Fig. 6). A combination of inverse tangential longitudinal strain (Ramsay & Huber 1987, p.448) and of pure shear strain (due to hinge-thickening as the incompetent layers take on a class 3 geometry) is adopted. For every considered folding stage, the inverse tangential longitudinal strains (implying shortening in the outer arc and extension in the inner arc) are assumed to be equal to the tangential longitudinal strains correspondingly developed in the competent layers. The deformation gradient tensors are therefore given by equation (6a) for the inner arc, and by equation (6b) for the outer arc. The pure shear strain arising from the thickening of the fold hinge is a simple function of layer thickness; the relative deformation matrix (constant throughout the whole hinge zone) is represented by equation (8). The volume changes accompanying tectonic deformation are assumed to occur by displacements along the x axis (parallel to the layering), since this represents the shortening direction for both the strain fields applied. The volume change deformation matrix is given by:

$$D = \begin{bmatrix} (1 + \Delta_i) & 0 \\ 0 & 1 \end{bmatrix}. \quad (12)$$

For every 5° increment of fold-limb dip, the total deformation gradient tensor is given by the multiplication of terms (6b), (8) and (12) for the outer arc, of (8) and (12) for the mid arc, and of (6a), (8) and (12) for the inner arc. These are all diagonal matrices (representing irrotational strains), and the order of matrix multiplication is in this case irrelevant.

DISCUSSION

Finite strain development in the model

The orientation and magnitude of the principal strains of the total deformation ellipsoid have been determined for every 5° increment of fold-limb dip. The deformation paths for the different parts of the deforming body analysed in the model are represented on the logarithmic deformation plot (Ramsay 1967, p. 138); the orthogonal axes are given by: $\ln(Y_f/Z_f) = \varepsilon_2 - e_3$ (abscissa), and $\ln(X_f/Y_f) = \varepsilon_1 - \varepsilon_2$ (ordinate), where $X_f > Y_f > Z_f$ are the lengths of the principal axes of the total finite strain ellipsoid (Figs. 8, 9 and 10).

In both competent and incompetent layers, the uniaxial compaction is represented by an oblate spheroid with $X_f = Y_f = 1$ parallel to the layering and $Z_f = (1 + \Delta_0) < 1$ vertical. This deformation plots on the abscissa axis at a point (dependent on the considered amount of compaction): $\varepsilon_2 - \varepsilon_3 = -\ln(1 + \Delta_0)$.

(*a*) *Competent layers.* In the competent layers, on application of pure shear strain due to initial layer-parallel shortening, the deformation path moves along a straight line with negative slope towards the prolate field (without entering it because of the low value of initial layer-parallel shortening employed for the model; Fig. 8). The total finite strain is at this stage quite small ($R_{xz} = 1.07$), and is characterized by a maximum principal strain ($X_f = 1$) parallel to the y axis of the reference frame. No further deformation occurs in the limbs and in

the mid arc of the hinge regions of folded competent layers (Fig. 8b). Tangential longitudinal strain produces instead the superposition of further pure shear increments in the inner arc and outer arc of the hinge regions.

In the inner arc, the shortening due to tangential longitudinal strain during folding acts in the same direction as the initial layer-parallel shortening; the deformation path moves into the field of apparent constriction (Fig. 8c). During these stages, the maximum principal strain ($X_f = 1$) is parallel to the y axis and the minimum principal strain is vertical. After the uniaxial prolate state is reached, there is a changeover in the positions of minimum and intermediate principal strains, but the maximum apparent extension parallel to the y axis is maintained as the deformation proceeds back along the same straight line from the prolate towards the oblate field to a shape identical to that after compaction alone. On application of further deformation increments there is an interchange of the intermediate and the maximum principal strains, and the deformation ellipsoid from now on is characterized by: $X_f > 1$ vertical, $Y_f = 1$ parallel to y, $Z_f < 1$ parallel to x.

In the outer arc of the hinge regions, the shortening direction of the tangential longitudinal strain during folding is parallel to that of the compaction. After the initial layer-parallel shortening counteracting the compactional deformation, the deformation path moves back towards the abscissa axis, due to the effect of stretching parallel to the x axis and renewed shortening along the z direction (Fig. 8a); the maximum principal strain ($X_f = 1$) is parallel to the y axis, whereas $Y_f < 1$ is parallel to x and $Z_f < 1$ is parallel to z. After the uniaxial oblate state is reached again, the maximum and intermediate principal strains changeover, and the deformation ellipsoid for the next strain increments is characterized by the coincidence of $X_f > 1$, $Y_f = 1$ and $Z_f < 1$ with the co-ordinate axes x, y and z, respectively.

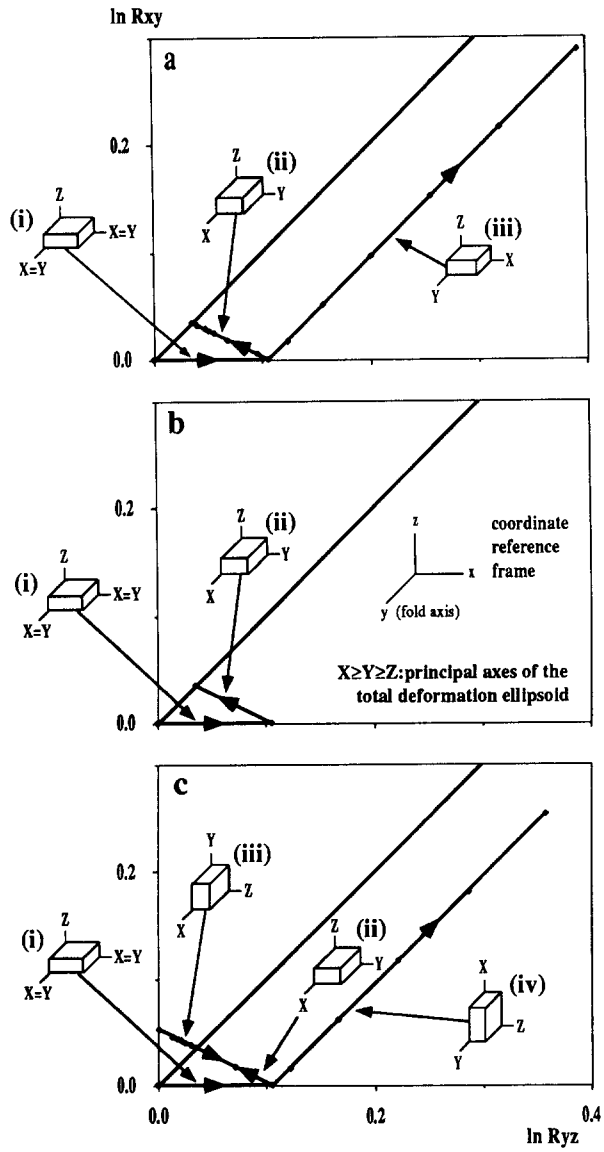

Fig. 8. Deformation paths for different parts of the competent layers in the model (10% initial compaction, no incremental volume change during tectonic deformation). (a) Hinge regions, outer arc. (b) Limb regions, and mid arc of the hinge regions. (c) Hinge regions, inner arc. In (b) the simple deformation path results from the superposition of compaction and uniform layer-parallel shortening, with no further deformation during fold development. In (a) and (c) a tangential longitudinal strain component during folding is considered. Data points represent 5° increments of fold-limb dip. The co-ordinate reference frame is given in (b). X, Y and Z on small cartoons refer to principal strain axes ($X = X_f$, $Y = Y_f$, $Z = Z_f$).

(*b*) *Incompetent layers.* In the incompetent layers, the superposition of compaction and initial layer-parallel shortening also produces a maximum extension parallel to the y axis, although no stretch occurs in this direction; the deformation path moves towards the apparent constriction field, but is still far from entering it (Figs. 9 and 10).

For the limb regions of folded incompetent layers, the whole deformation path lies in the apparent flattening field (Figs. 9a and 10a). During the first stages of fold development, the apparent maximum extension parallel to the y direction is maintained in the limbs as the deformation path proceeds back towards the abscissa axis. After the uniaxial oblate state is reached, the intermediate and the maximum principal strains changeover, the intermediate principal strain becoming parallel to the y axis. A maximum extension parallel to the fold axis characterises the limb regions during the early folding stages; as folding proceeds, the maximum principal strain changes direction through 90° to lie within the plane normal to the fold axis. Another interesting feature predicted from the model is the small angle between the XY plane of the total deformation ellipsoid and the layering in the fold limbs, due to the effects of previous compaction; this angle is much less variable than that predicted for tectonic deformation alone (Fig. 11).

In the fold hinge regions, the coaxial strains considered in the model lead to an apparent maximum extension more persistently parallel to the y axis (Figs. 9b–d and 10b–d). During the first tectonic strain increments, the deformation path proceeds from the oblate to the prolate field and the deformation ellipsoid is characterized by $X_f = 1$ parallel to y and Z_f vertical. After the uniaxial prolate state is reached, the deformation returns towards the apparent flattening field (without following the same path because of the effects of in-

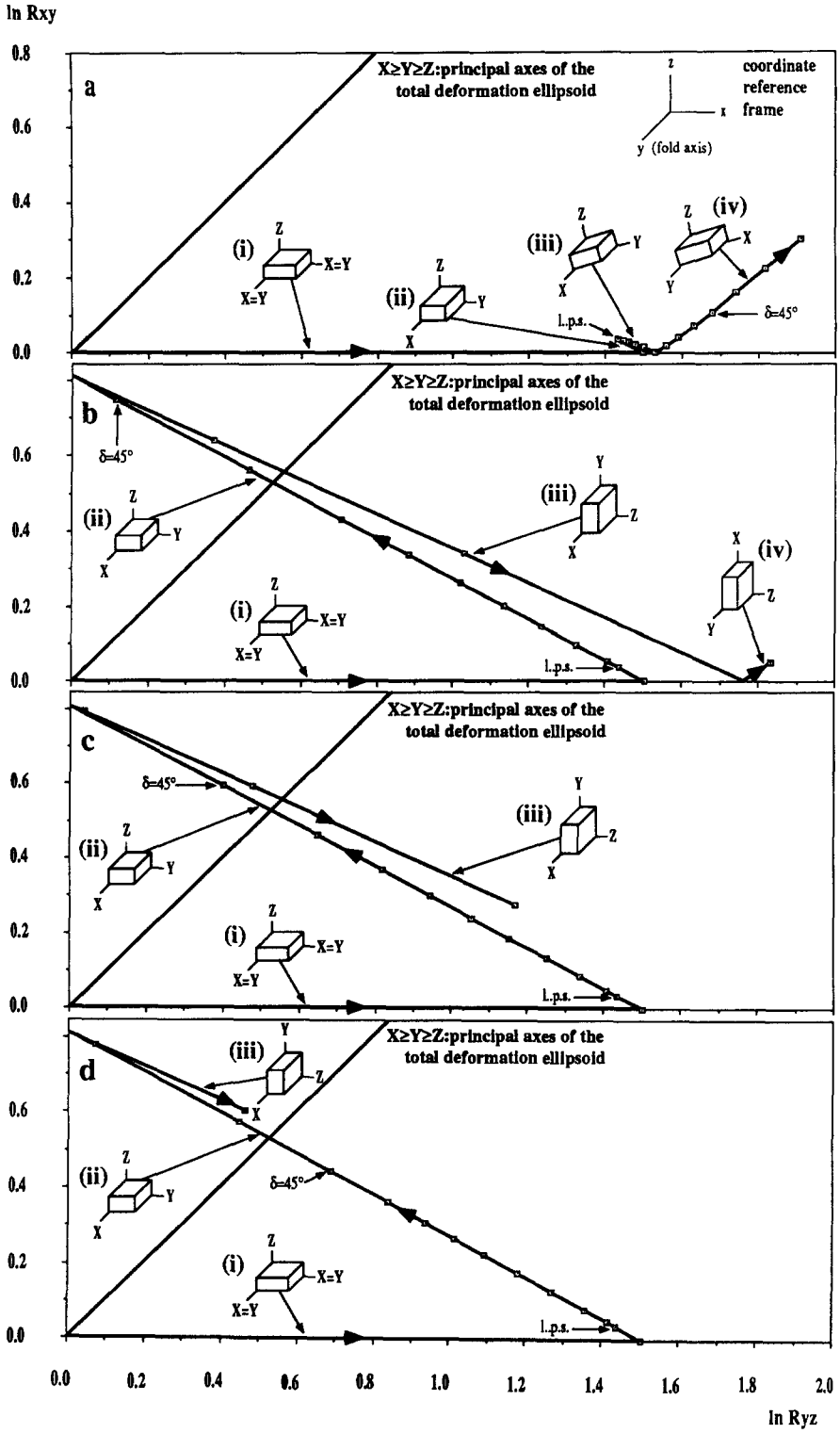

Fig. 9. Deformation paths for different parts of the incompetent layers in the model (78% initial compaction, incremental volume change during tectonic deformation). (a) Limb regions. (b) Hinge regions, outer arc. (c) Hinge regions, mid arc. (d) Hinge regions, inner arc. Data points represent 5° increments of fold-limb dip.

cremental volume change during tectonic deformation); during these stages, the maximum principal strain ($X_f = 1$) remains parallel to the y axis, but the minimum and the intermediate principal strains interchange so that Z_f becomes parallel to the tectonic shortening direction (x axis). When the uniaxial oblate state is eventually reached, the principal axes of the strain ellipsoid switch again; for any further deformation increment the axes of total strain coincide with those of tectonic strain, being: $X_f > 1$ vertical, $Y_f = 1$ parallel to y, $Z_f < 1$ parallel to x. A maximum stretching parallel to the fold axis therefore characterizes the hinge region for most of its deformation history, and only when relatively high shortening values are reached (50% in the mid arc region for the case of 55% compaction) does the maximum principal strain axis take on a vertical position. Another interesting feature predicted from the model is the occurrence of prolate strains in the hinge regions of

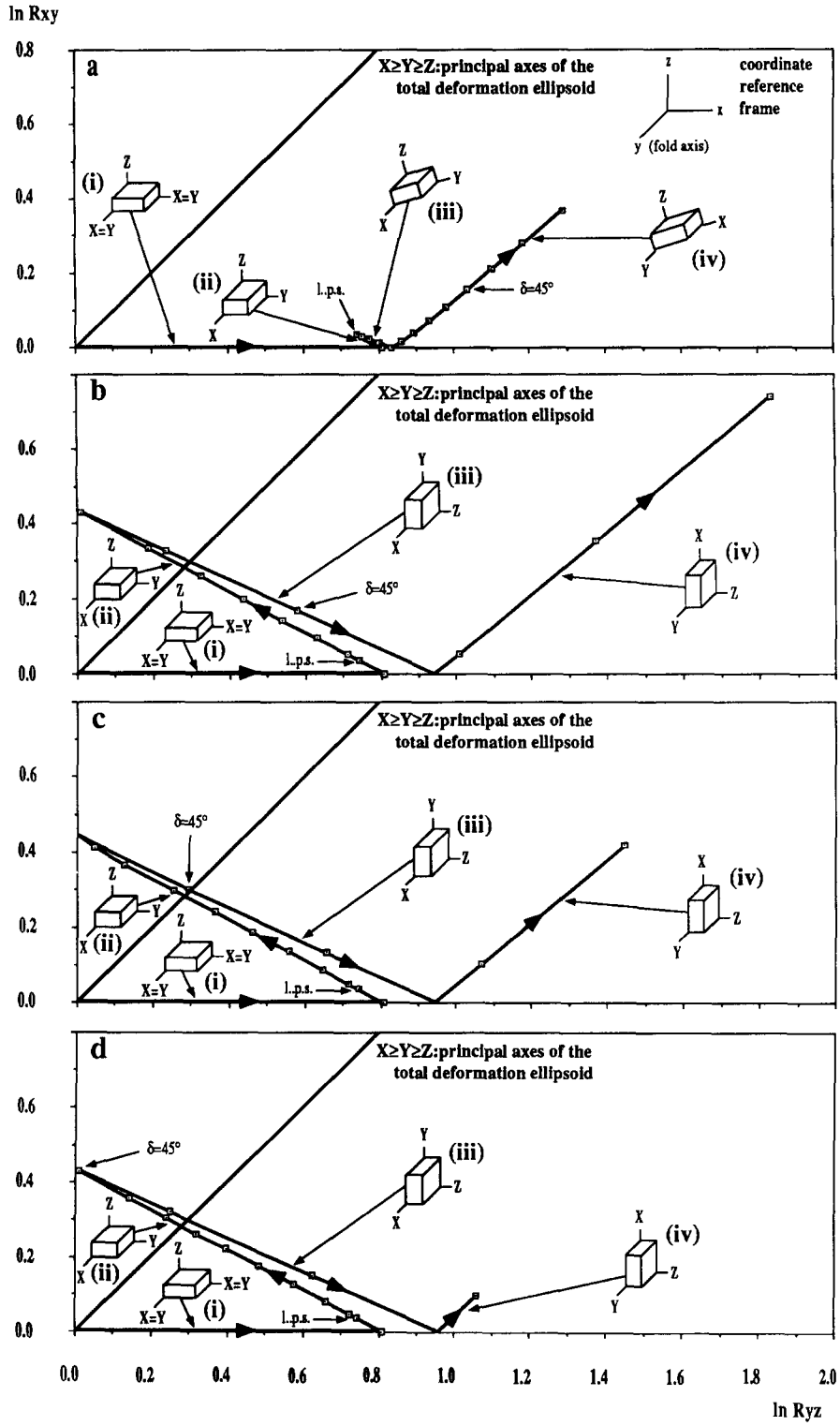

Fig. 10. Deformation paths for different parts of the incompetent layers in the model (55% initial compaction, incremental volume change during tectonic deformation. (a) Limb regions. (b) Hinge regions, outer arc. (c) Hinge regions, mid arc. (d) Hinge regions, inner arc. Data points represent 5° increments of fold-limb dip.

open folds: for instance, constrictional strains characterize the mid arc region for folding stages between 20 and 36% shortening (corresponding to limb dips of 30–45°) in the case of 55% initial compaction (Fig. 10c).

The effects of the inverse tangential longitudinal strain component considered in the model result in deformation paths proceeding more rapidly from the inner to the outer arc of the hinge regions; consequently, for some folding stages the coexistence of prolate strains in the inner arc and oblate strains in the outer arc is predicted (Fig. 12).

Comparison with field observations: planar and linear fabrics in the Galestri Formation, Lagonegro zone, Southern Apennines

A field study of fabric development in relation to position within folds has been carried out in interbedded

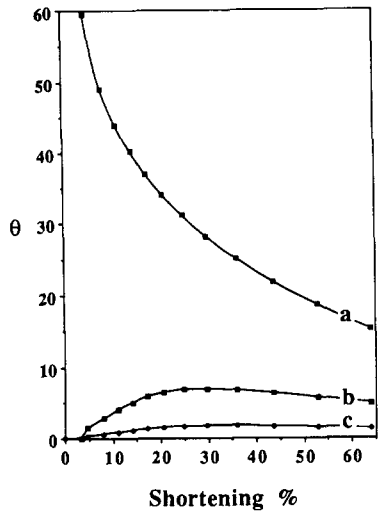

Fig. 11. Orientation (θ) of the XY plane of the deformation ellipsoid with respect to bedding in the limb regions of folded incompetent layers: a = tectonic XY plane; b = total XY plane for 55% compaction; c = total XY plane for 78% compaction. Note the much reduced variability of the angle θ due to the effect of diagenetic compaction (curves b and c).

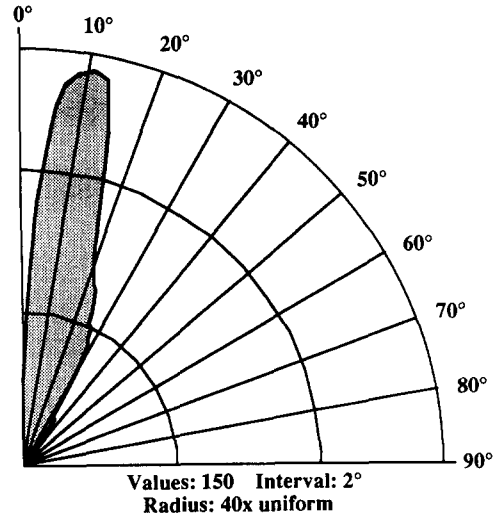

Fig. 13. Angle between cleavage and bedding in folded argillites of the Lower Cretaceous Galestri Formation (Lagonegro area, Southern Apennines). Data are from folds varying from open to tight; values in the range 5–15° are largely dominant, irrespective of the degree of tightness of the folds.

argillites and siliceous limestones of the Galestri Formation of the Lagonegro area (Fig. 1). Depending on the position within mesoscopic folds and on fold shape, different types of planar and linear fabrics occur in the incompetent argillites.

In the fold-limb regions, the argillites usually display a well-developed planar fabric that makes a small, but still detectable angle with the bedding surfaces (5–15° being typical; Figs. 13 and 16a,b & d). Cleavage at a low angle to bedding is recorded from a large variety of folds, irrespective of their degree of tightness. This feature shows a clear analogy with the orientation of the XY plane of the total finite strain ellipsoid predicted from the model (Fig. 11). A more accurate comparison, involving the reconstruction of the total deformation ellipsoid by means of strain analysis, was in the present case not possible because of the lack of suitable strain markers in the argillites. On the other hand, cleavage in these rocks is of continuous (slaty) type and is defined exclusively by a preferred dimensional orientation of phyllosilicate grains (Fig. 16d & e). This type of foliation, lacking planar discontinuities, may be expected to develop parallel to the XY plane of strain and to 'track' that plane during a non-coaxial strain history such as that generally occurring in fold limbs (Williams 1976).

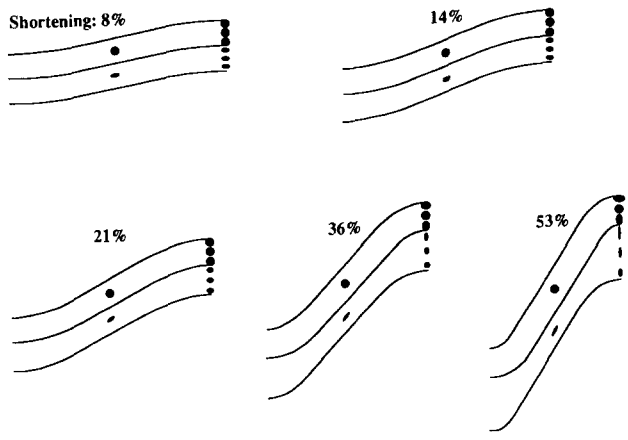

Fig. 12. Total finite strain developed in fold profile for some of the folding stages of the model. Initial compaction of the incompetent layers: 55%. Strain ellipses are scaled for volume changes.

In the hinge zone of open folds, the incompetent layers often display a linear pencil fabric sub-parallel to the fold axis (Fig. 14). The pencils have cross-sectional shapes bounded by irregular polygonal or curvilinear walls (Fig. 17a), and show no distinct planar fabric anisotropies in outcrop (Fig. 17b). They are considered to be 'true' pencil structures in the sense of Ramsay & Huber (1983, pp. 185–186), representing a linear fabric element associated with a prolate finite strain in the material. A different fabric can be generally observed in the hinge region of close folds, where a spaced cleavage occurs in association with a more regular pencil structure sub-parallel to the fold axis (Fig. 15). The pencils show a rectangular profile, with cleavage surfaces being dominant (Fig. 17c). This fabric is likely to represent an oblate finite strain in the rock, although the tectonic strain imprint at this stage has not been sufficiently strong to induce the complete acquisition of a true planar fabric. On a few occasions, a transition from a linear pencil fabric in the inner arc to a weak planar fabric in the outer arc can be observed. By analogy with the model (Fig. 12), this transition is likely to be due to an inverse tangential longitudinal strain component. A well-developed slaty cleavage, slightly divergent or sub-parallel to the fold axial surfaces, can conversely be observed in tightly to isoclinally folded argillites (Fig. 17d).

CONCLUSIONS

The superposition of plane strain on a uniaxial flattening is used as a simple model for finite strain

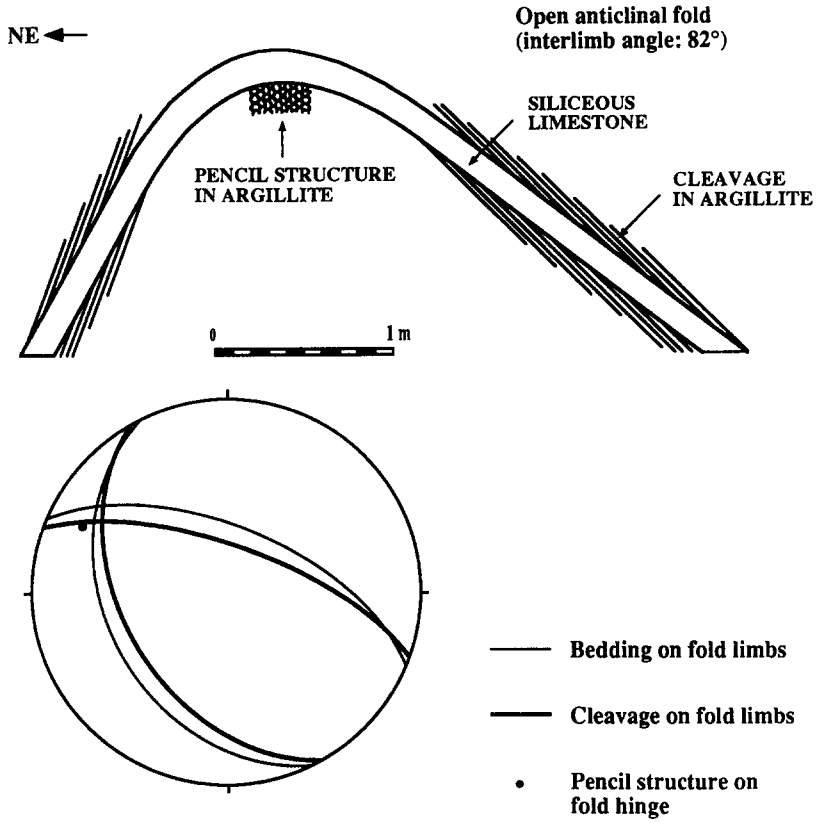

Fig. 14. Field example of an open anticlinal fold in argillites and interbedded siliceous limestones of the Galestri Formation (Lagonegro area, Southern Apennines). Note cleavage is at a low angle to bedding on the fold limbs, and 'true' pencil structure occurs in the fold hinge.

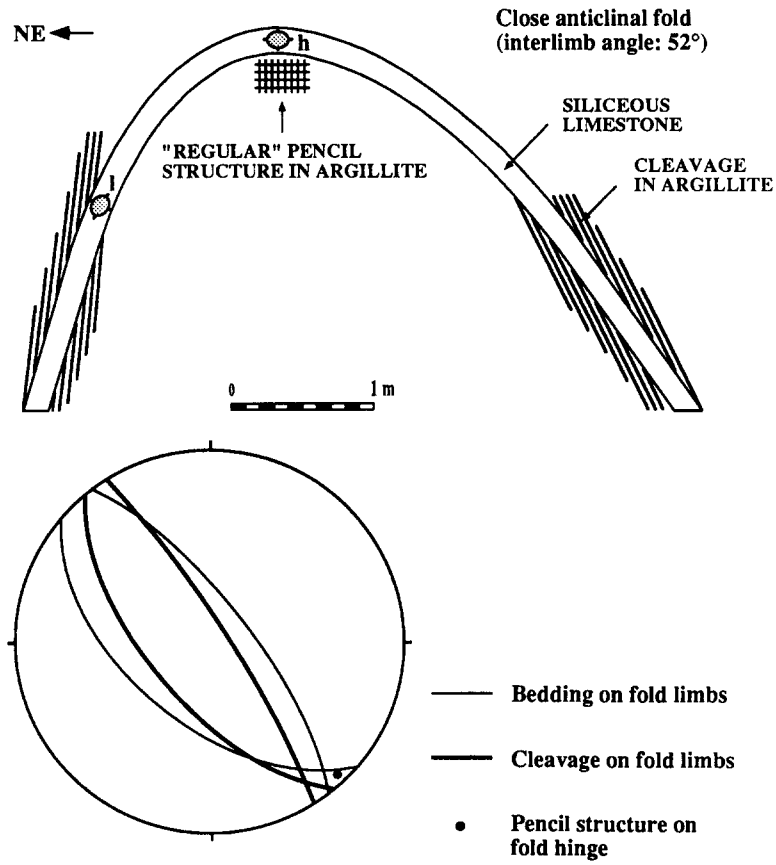

Fig. 15. Field example of a close anticlinal fold in argillites and interbedded siliceous limestones of the Galestri Formation (Lagonegro area, Southern Apennines). Note cleavage at a low angle to bedding on the fold limbs, and 'regular' pencil structure in the fold hinge. In the limestone layer, strain ellipses determined from R_f/ϕ analysis on deformed radiolarians are shown; maximum shortening directions make an (anticlockwise) angle of 89° and 81° with bedding in the hinge (h) and limb (1) regions, respectively.

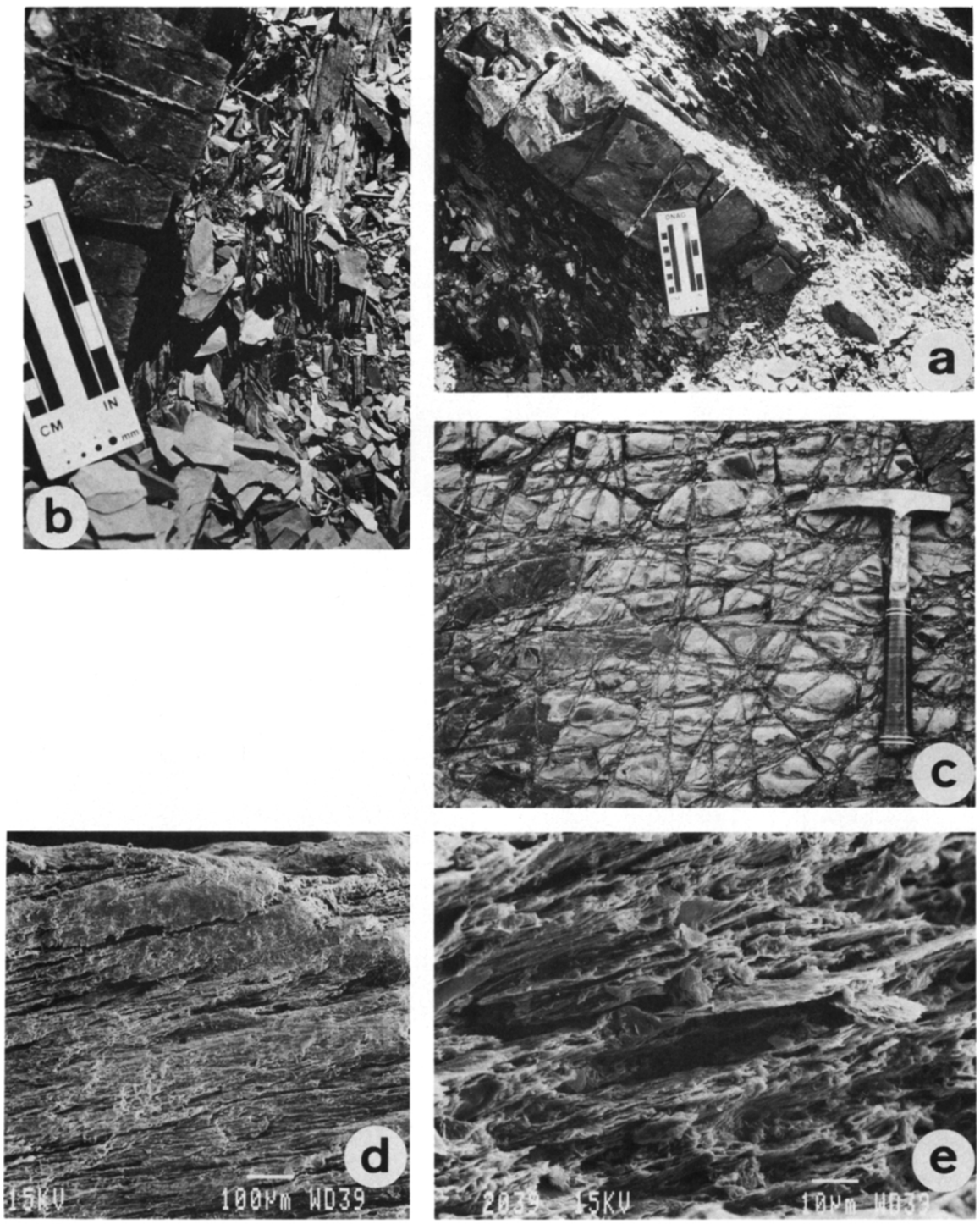

Fig. 16. (a) Southwestern limb of the anticline of Fig. 14, showing slaty cleavage at a low angle to bedding in the argillites. (b) Detail of the northeastern limb of the anticline of Fig. 14, showing slaty cleavage in the argillite. Calcite-filled veins approximately normal to bedding in the limestone layer belong to different fracture sets shown in (c). (c) Fracture pattern on the bedding surface of a limestone layer (fold axis in the picture is oriented horizontally). The origin of these fracture systems in folds is discussed in Price & Cosgrove (1990, pp. 378–383). (d) SEM micrograph of slaty cleavage at a low angle to bedding (horizontal top surface) in the argillites. (e) SEM micrograph showing cleavage fabric defined by homogeneous alignment of clay platelets.

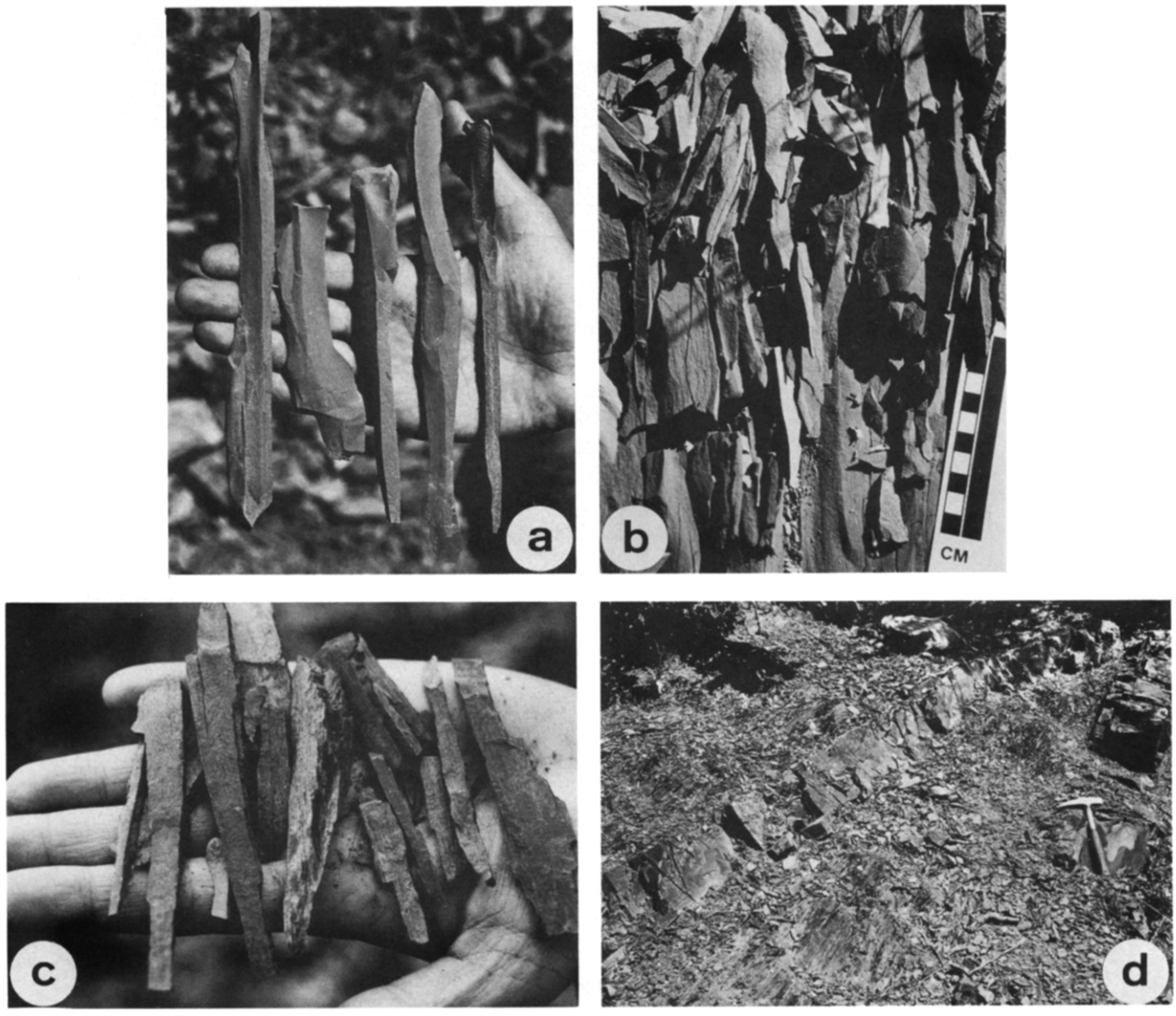

Fig. 17. (a) 'True' pencils (bounded by irregular curvilinear surfaces) in argillite. (b) 'True' pencil structure (showing no distinct planar fabric anisotropies) in outcrop. (c) 'Regular' pencils from the hinge region of the anticline of Fig. 15. The two dominant surfaces of the pencils represent cleavage surfaces. (d) Tight anticlinal fold in argillites and interbedded siliceous limestones of the Galestri Formation (Lagonegro area, Southern Apennines); slaty cleavage is sub-parallel to the fold axial surface.

development during folding of a previously compacted multilayer sequence. Different parts of the deforming body in the model show complex deformation paths, with the principal axes of the total deformation ellipsoid interchanging their position several times during fold development.

A quantitative comparison between the strain states predicted from the model and those acutally occurring in the incompetent beds in the field was in the present case not possible because of the lack of strain markers in the argillites. Nevertheless, planar and linear fabrics developed in different parts of individual folds are an expression of such strain states (Reks & Gray 1983), and allow a sound analysis to be made. In this sense, finite strain states predicted from the model appear to be in good agreement with observations of fabric development in naturally deformed rocks from the Southern Apennines. In particular, it can be seen that:

(1) during progressive deformation in the model, the finite strain ellipsoid in the limb regions of folded incompetent layers is consistently oblate, and its XY plane lies at a small angle to bedding as a consequence of previous compaction. It can be envisaged that the cleavage at a low angle to bedding observed in the field in the argillites represents the XY plane of the total deformation ellipsoid in strongly compacted sediments, and not that of tectonic deformation alone;

(2) finite strains predicted in the incompetent layers of the model are of prolate type in the hinge regions of open folds, and become oblate as the interlimb angle decreases; the presence of 'true' pencil structures in open folds and of a spaced cleavage associated with 'regular' pencil structures in more close folds, often noted in the case study of the Southern Apennines, most probably reflects this change from prolate to oblate strain in the hinge zones as folding proceeds.

It can also be noted that the hinge zone of folded incompetent layers in the model develops a maximum stretching parallel to the fold axis for most of its deformation history. Consistent finite extensions parallel to the fold axis may therefore be recorded from (compaction sensitive) strain indicators in compacted rocks, although very little or no stretch has actually occurred along this direction.

Acknowledgements—We are grateful to John Ramsay for suggesting this project, and for stimulating discussions while preparing the manuscript. Many thanks to Dorothee Dietrich and Neil Mancktelow for critically reading the manuscript. Critical comments by Mary Ford, Norman Fry and Jean-Pierre Gratier helped to improve this paper. We would also like to thank our colleagues Djordje Grujic and Giorgio Pennacchioni for their useful comments and Urs Gerber for prints of the photographic material. Financial support from the ETH Zürich is gratefully acknowledged. S.M. acknowledges the financial support of CNR contribution No. 11 (responsible F.-C. Wezel) during the first year of his stay in Zürich.

REFERENCES

Beutner, E. C. & Charles, E. G. 1985. Large volume-loss during cleavage formation, Hamburg sequence, Pennsylvania. *Geology*, **13**, 803–805.

Burst, J. F. 1969. Diagenesis of Gulf Coast clayey sediments and its possible relation to petroleum migration. *Bull. Am. Ass. Petrol. Geol.* **53**, 73–93.

Coogan, A. H. & Manus, R. W. 1975. Compaction and diagenesis of carbonate sands. In: *Compaction of Coarse-grained Sediments, I, Developments in Sedimentology, Vol.* 18A (edited by Chilingarian, G. V. and Wolf, K. H.). Elsevier, Amsterdam, 79–176.

Engelder, T. & Geiser, P. 1979. The relationship between pencil cleavage and lateral shortening within the Devonian section of the Appalachian Plateau, New York. *Geology* **7**, 460–464.

Engelder, T. & Marshak, S. 1985. Disjunctive cleavage formed at shallow depths in sedimentary rocks. *J. Struct. Geol.* **7**, 327–343.

Hudleston, P. & Tabor, J. 1988. Strain and fabric development in a buckled calcite vein and rheological implications. *Bull. geol. Instn Univ. Uppsala* **14**, 79–94.

Huggenberger, P. 1985. Faltenmodelle und Verformungsverteilung in Deckenstrukturen am Beispiel der Morcles-Decke (Helvetikum der Westschweiz). Unpublished Ph.D.thesis, Geologisches Institut, ETH, Zürich, Switzerland.

Müller, G. 1967. Diagenesis in argillaceous sediments. In: *Diagenesis in sediments, Developments in Sedimentology, Vol.* 8 (edited by Gunnar, L. & Chilingarian, G. V.). Elsevier, Amsterdam, 127–177.

Pozzuoli, A., Scandone, P., Huertas, F. & Linares, J. 1977. Risultati preliminari dello studio sui minerali argillosi triassici del Bacino Lagonegrese (Lucania, Appennino Meridionale). *Geol. appl. idrogeol. Bari* **12**, 109–121.

Price, N. J. & Cosgrove, J. W. 1990. *Analysis of Geological Structures*. Cambridge University Press, Cambridge.

Ramsay, J. G. 1967. *Folding and Fracturing of Rocks*. McGraw-Hill, New York.

Ramsay, J. G. & Huber, M. I. 1983. *The Techniques of Modern Structural Geology, Volume* 1: *Strain Analysis*. Academic Press, London.

Ramsay, J. G. & Huber, M. I. 1987. *The Techniques of Modern Structural Geology, Volume* 2: *Folds and Fractures*. Academic Press, London.

Ramsay, J. G. & Wood, D. S. 1973. The geometric effects of volume change during deformation processes. *Tectonophysics* **16**, 263–277.

Reks, I. J. & Gray, D. R. 1982. Pencil structure and strain in weakly deformed mudstone and siltstone. *J. Struct. Geol*, **4**, 161–176.

Reks, I. J. & Gray, D. R. 1983. Strain patterns and shortening in a folded thrust sheet: an example from the southern Appalachians. *Tectonophysics* **93**, 99–128.

Rieke III, H. H. & Chilingarian, G. V. 1974. *Compaction of Argillaceous Sediments, Developments in Sedimentology, Vol.* 16. Elsevier, Amsterdam.

Sanderson, D. J. 1976. The superposition of compaction and plane strain. *Tectonophysics* **30**, 35–54.

Scandone, P. 1972. Studi di geologia lucana: Carta dei terreni della serie calcareo-silico-marnosa e note illustrative. *Soc. natur. Napoli Boll.* **81**, 225–300.

Scandone, P. 1975. The preorogenic history of the Lagonegro basin (Southern Apennines). In: *Geology of Italy* (edited by C. Squyres). Earth Sciences Society of the Lybian Arab Republic. Tripoli.

Von Engelhardt, W. 1960. *Der Porenraum der Sedimente*. Springer Berlin.

Weller, J. M. 1959. Compaction of sediments. *Bull. Am. Ass. Petrol. Geol.* **43**, 273–310.

Williams, J. R. 1980. Similar and chevron folds in multilayers using finite-element and geometric models. *Tectonophysics* **65**, 323–338.

Williams, P. F. 1976. Relationship between axial-plane foliations and strain. *Tectonophysics* **30**, 181–196.

Wolf, K. H. & Chilingarian, G. 1976. Diagenesis of sandstones and compaction. In: *Compaction of Coarse-grained Sediments, II, Developments in Sedimentology, Vol.* 18B (edited by Chilingarian, G. & Wolf, K. H.). Elsevier, Amsterdam, 69–444.

Wood, D. S. 1974. Current views of the development of slaty cleavage. *Annu. Rev. Earth & Planet. Sci.* **2**, 369–401.

Wright, T. O. & Henderson, J. R. 1992. Volume loss during cleavage formation in the Meguma Group, Nova Scotia, Canada. *J. Struct. Geol.* **14**, 281–290.

Wright, T. O. & Platt, L. B. 1982. Pressure dissolution and cleavage in the Martinsburg Shale. *Am. J. Sci.* **282**, 122–135.